Magnetic Hyperfine Interaction of Cr^{53}†

W. J. CHILDS, L. S. GOODMAN, AND D. VON EHRENSTEIN
Argonne National Laboratory, Argonne, Illinois
(Received 18 July 1963)

The hfs of Cr^{53} has been investigated by the atomic-beam magnetic-resonance technique. The atoms were detected with an electron-bombardment universal detector. Novel counting techniques made possible observation of resonances for which the signal-to-background ratio was 0.0002. The magnetic-dipole hyperfine-interaction constant was measured to be $a=\pm(82.5985\pm0.0015)$ Mc/sec and the electric-quadrupole hyperfine-interaction constant was found to be consistent with $b=0$. These results are compared with the theory. From the measured value of a, the average magnetic field at the nucleus is calculated to be 1.03×10^6 G within about 1%.

I. INTRODUCTION

THE initial motivation for this experiment was provided from work carried out at this laboratory on the isotope Cr^{51}. Since the magnetic hyperfine interaction constant a and the nuclear spin I for[1] radioactive Cr^{51} and the magnetic moment μ_I and I for[2] Cr^{53} had already been measured, it is clear that a measurement of a for Cr^{53} was all that was lacking in order to make a good estimate of μ_I for Cr^{51}.

The hfs of Cr^{53} is itself of interest. As discussed below, the measured value of a differs considerably from the theoretical value inferred from the measured value of the magnetic moment. It is to be hoped that the eventual resolution of this discrepancy will lead to improved understanding of hfs calculations.

The results given here are for Cr^{53}; a full report on Cr^{51} will be published later.

II. APPARATUS

The atomic-beam magnetic-resonance machine used for the present experiment is new. Since a complete description will be published later, only a brief account will be given here.

The basic machine is of the conventional Rabi-Zacharias[3] type with 2-pole inhomogeneous fields which have their gradients in the same direction. The distance from the oven slit to the detector slit is 52.5 cm. The inhomogeneous fields are sustained by permanent magnets, may be operated up to 21 kG, and can easily be energized, de-energized, or set at intermediate strengths. In order to adjust the field strengths (and, hence, the field gradients) of the two to achieve good refocusing, Hall element magnetometers are used to measure the fringing fields near the magnet legs.

The C field is 10.4 cm long and is equipped with 4 rf loops, one of which may be rotated 90° to change the direction of the rf magnetic field relative to the uniform field.

The tantalum oven holder, operated at a high positive voltage, is heated by electron bombardment from grounded filaments. The total power drawn is regulated by a Hall element which senses the product of the voltage and the emission current. The oven system is surrounded by a water-cooled copper jacket.

Provision is made for lateral movement and tilt of the detector and collimator slits, the oven, and the obstacle wire.

The detection system used (discussed below) requires that the vacuum in the machine be extremely clean. The vacuum system is of nonmagnetic stainless steel throughout, and all vacuum seals are made with gold gaskets with the exception of a very few O-rings in the oven section. The oven system is pumped with a 1600-liter/sec mercury pump with refrigerated baffle and liquid nitrogen trap, and the detector and differential (buffer) systems are pumped with commercial ion-getter pumps. The vacuum in the detector section is normally below 1×10^{-7} mm Hg when the electron-bombardment detector is operating. A liquid nitrogen trap keeps the detector surfaces cold. The mass spectrum of the detector vacuum is rather free from background at most masses. The electron-bombardment universal detector will be discussed separately below.

With the universal detector and its associated counting and modulating circuitry, both "flop-in" and "flop-out" transitions can be detected. Flop-in transitions are observed when atoms undergo a change of state bebetween the inhomogeneous fields such that their deflection in one magnet is exactly cancelled by that in the other. Under these conditions, the atom passes through the detector slit and is counted. Since more are counted when the rf is "on" than when it is "off," the atoms undergoing the transition are said to have been flopped in. Flop-out transitions result when atoms pass through the first inhomogeneous magnet with no effective magnetic moment (and, hence, are undeflected) but subsequently undergo a transition to a state in which they can be deflected away from the detector. Since applica-

† Work performed under the auspices of the U. S. Atomic Energy Commission.

[1] W. J. Childs, L. S. Goodman, and L. J. Kieffer, Bull. Am. Phys. Soc. **3**, 151 (1959). Results of further work will be published.

[2] B. Bleaney and K. D. Bowers, Proc. Phys. Soc. (London) **A64**, 1135 (1951); F. Alder and K. Halbach, Helv. Phys. Acta **26**, 426 (1953); C. D. Jeffries and P. B. Sogo, Phys. Rev. **91**, 1286 (1953). The moment has been corrected for diamagnetic shielding according to W. C. Dickenson, Phys. Rev. **80**, 563 (1950).

[3] I. I. Rabi, J. R. Zacharias, S. Millman, and P. Kusch, Phys. Rev. **53**, 318 (1938); J. R. Zacharias, Phys. Rev. **61**, 270 (1942).

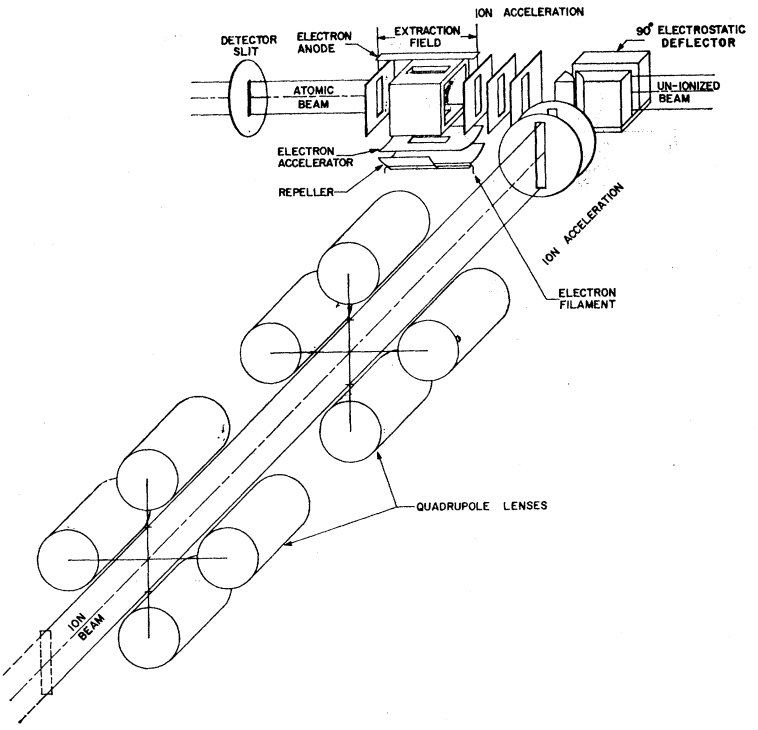

FIG. 1. Schematic diagram of the electron-bombardment universal detector. The atomic beam, after passing through the detector slit, is partially ionized in the ion box, which is at a high positive voltage V_0. The box is kept at liquid nitrogen temperature. The ions produced, including those due to the bombardment of the rest gas, are swept out of the ion box in the direction of the beam. After acceleration through about 0.4 V_0, they are deflected through 90° in an electrostatic deflector and further accelerated to ground. The functioning of the electrostatic quadrupole lenses is described in the text. The electron beam is produced by a Pierce gun.

tion of the appropriate rf signal causes fewer atoms than normal to be counted, such a transition is termed a flop-out transition.

When observing flop-in transitions, it is often convenient to place an obstacle wire on the machine axis near where the atoms undergo maximum off-center deflection. This renders the machine geometrically opaque but does not affect the strength of the resonance signal appreciably. It is clear, however, that such an obstacle cannot be used when flop-out transitions are of interest. No obstacle was used in the present experiment.

The Electron-Bombardment Universal Detector

Those atoms of the beam which go through the detector slit continue along the machine and pass through the ion-source chamber of a mass spectrometer. While in this chamber, the atoms are subjected to a bombardment of electrons from a Pierce gun. The electrons are accelerated vertically, perpendicular to the velocity of the atoms and parallel to the slits which define the ribbon-shaped atomic beam. The arrangement is shown schematically in Fig. 1.

The atoms that are ionized are accelerated out of the ion source by an electric field in the direction of the atomic beam. This field is produced by applying a voltage between the insulated end plates of the source chamber. The ions are further accelerated, electrostatically deflected by means of a 90° deflector, and then given additional acceleration to ground potential.

Before entering the deflecting magnet of the mass spectrometer, the ions pass through a pair of electrostatic quadrupole lenses which serve three purposes. (1) The horizontal components of the ion velocities are made parallel so as to satisfy the focusing conditions of the mass spectrometer. (2) The ion paths are caused to converge vertically toward the horizontal mid-plane to improve the transmission through the magnet chamber of the mass spectrometer. (3) A bias voltage can be applied to the electrodes so that the quadrupole lens system also serves as a deflector which corrects for any accidental misalignment of the ion beam in the vertical direction.

The ions are detected at the focus of the mass spectrometer by use of a DuMont SP-123 electron-multiplier assembly in conjunction with a fast pulse-counting system.

Although the mass spectrometer (which has a 12.5-in. radius of curvature) is capable of fairly good resolution, this feature was not used in the present experiment. For the purposes of this experiment the defining slit was removed from the machine, and the full $\frac{1}{2}$-in. width of the first dynode of the electron multiplier was exposed directly to the focused beam of ions. This reduced the resolution so that masses 52 and 53 of the chromium beam were quite unresolved and could be detected simultaneously. The mass spectrometer had to be in this manner so that Cr^{52} and Cr^{53} resonances could be observed simultaneously with the same detection system.

This type of operation has four interesting conse-

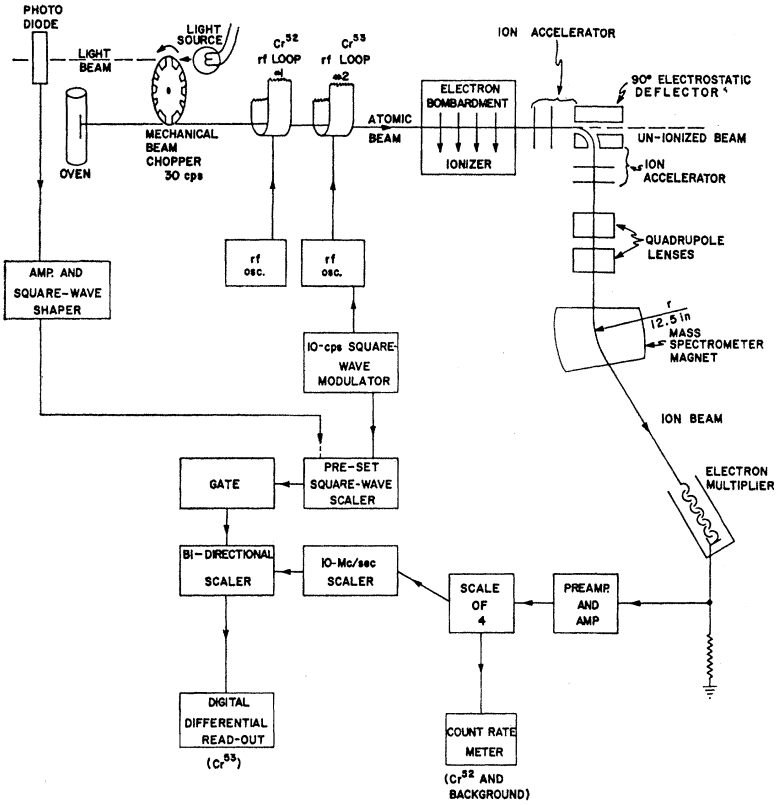

FIG. 2. Block diagram of the detector electronics. The atomic beam is represented at the top of the figure. The electron bombardment detector is shown at the upper right. The outputs of the circuit appear at the bottom.

quences. (1) The efficiency for detecting the beam is enhanced. (2) The performance of the detection system is very stable since drifts of the magnetic field or accelerating voltage are relatively less important than for operation with high resolution. (3) The ion source can be operated at conditions of maximum detected beam without thought as to how adversely this affects the resolution. (4) The background signal is increased.

Although the ion source itself is of rather conventional design,[4] a few features deserve mention. The source chamber (ion box) is made of soft iron to assist in the reduction of stray fields from the nearby B magnet. The field in the ion box with the B magnet fully energized (21 kG) is only 2—3 G. As a precaution, this iron box has been gold plated to reduce outgassing from the surface and to inhibit the buildup of insulating coatings which might impair the operation of the ion source. There is provision for heating the ion source with an auxiliary electron-bombardment system in order to bake it out. There has been no necessity for the use of this procedure so far.

The ion box has insulated end plates to which voltages can be applied to compensate for the potential well caused by the high-electron density produced by the Pierce gun and to accelerate the ions out of the source.

The ion box is bolted to a heavy copper block which is maintained at liquid nitrogen temperature. The liquid nitrogen reservoir may be filled without interrupting measurements. With the mass spectrometer adjusted to detect the chromium beam, filling the trap reduced the background by a factor of 20.

[4] G. Wessel and H. Lew, Phys. Rev. **92**, 641 (1953); G. Fricke, Z. Physik **141**, 166 (1955).

Electronic Counting System

A schematic diagram of the detector electronics is shown in Fig. 2. The pulses from the electron multiplier are fed to a fast preamplifier which is followed by a scale-of-four tunnel-diode circuit. The resolving time of this system is about 10 nsec. The output of this system is used to give a dc-analog counting rate on a meter and also to give shaped output pulses suitable for the input to a scaler. These shaped pulses are fed to a Berkeley model-7070R 10-Mc/sec scaler. Outputs from this scaler can be chosen to be 10^{-1} to 10^{-5} of the input counting rate. The output counts of the 10-Mc/sec scaler will be called the "scaled counts."

The scaled counts are fed into a control circuit which gates them alternately to the "add" and "subtract" channels of an Erie-500 T bidirectional scaler (bds). The gate is, in turn, controlled by a low-frequency square-wave generator. The counting time is determined by a preset scaler which counts the square-wave pulses. The time is always an integral number of full cycles of the square wave. This guarantees that the time spent in counting forward (in the add channel) is equal

to the time spent counting backward (in the subtract channel). When there is no synchronous modulation of the atoms arriving at the ion source, the bds should register zero within the statistical uncertainty determined by the counting rate.

The same square-wave generator is used both to gate the scaled counts and also to modulate the radio-frequency oscillator used to produce a resonance in the homogeneous magnetic field of the atomic-beam apparatus. Those atoms that undergo a radio-frequency transition in this field and are thus deflected into (away from) the ion source give rise to a net number of counts in the bds which is greater than (less than) zero.

This detection scheme can be used with quite small signal-to-background ratios. It is only necessary to accumulate counts long enough so that the number of detected ions representing the signal exceeds the square root of the background count by the desired signal-to-noise ratio.

Specifically, if s is the counting rate corresponding to the signal, b is the background rate, and t is the counting time, then the signal-to-noise ratio is $\eta = st/[(b+s)t]^{1/2}$. Hence, the counting time required to achieve the desired value of η is

$$t=\eta^2(b+s)/s^2. \tag{1}$$

A typical experimental case is shown in Fig. 3, a plot of a flop-out resonance in Cr^{53}. At resonance, the signal was 1800 sec^{-1}, while the total counting rate was $b+s=8\times10^6$ sec^{-1} so that the signal-to-background ratio was $s/b=0.022\%$. To achieve the desired signal-to-noise ratio $\eta=9$, the integrating time must be about 200 sec. In practice, the count at each ratio frequency was divided into several 30-sec intervals and the rates in these intervals were averaged. This allows detection of any extreme nonstatistical fluctuations due to counts introduced by momentary voltage breakdowns in the electrical systems of the oven or ion source, errors made by the counting equipment, etc.

At the peak of the Cr^{52} resonance observed with the same total counting rate, the signal was $s=1.5\times10^6$ sec^{-1}. Thus, for $\eta=100$, the required counting time was only $t=0.04$ sec. The Cr^{52} resonance signal was therefore easy to observe, without modulation, on the dc counting-rate meter.

Observation of undeflected (open) beams or nonresonant deflected beams was facilitated by mechanical modulation. This modulation was effected by means of a rotating toothed wheel inside the vacuum system. The wheel was driven by a motor outside the vacuum system via a magnetic clutch which transmitted the necessary torque through the vacuum wall. A similar toothed wheel outside the vacuum was driven by the same motor and was used to modulate a light beam incident on a photodiode. Pulses from the photodiode were then used to generate a square-wave signal synchronous with the square-wave modulation of the atomic beam. When this square wave was used to gate the inputs to the bds while the beam was being chopped mechanically, the atomic beam could be detected and conditions for this detection could be optimized, independently from the detection of ions due to non-beam-associated background. In what follows, such background will be referred to as "rest gas" background.

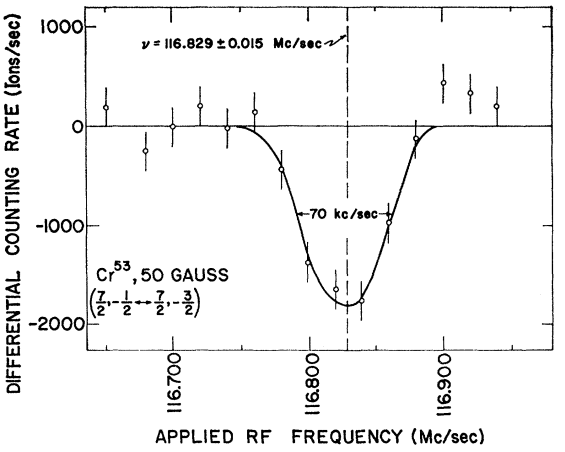

FIG. 3. The $(\frac{7}{2}, -\frac{1}{2} \leftrightarrow \frac{7}{2}, -\frac{3}{2})$ single-quantum flop-out transition ζ in Cr^{53} as observed at 50 G. The counting rate designated "0" is about 8×10^6/sec. The maximum signal observed is thus seen to be about 0.022% of the total counting rate and is only about 0.1% as intense as the Cr^{52} signal used to monitor the field. The counting time per point was 3–5 min.

III. THEORY

The Hamiltonian for a neutral atom in an external magnetic field H is separable so that the hyperfine-structure part may be considered independently. The hfs Hamiltonian is given (to sufficiently high order for the present experiment) by the expression[5]

$$\mathcal{H}=ha\mathbf{I}\cdot\mathbf{J}+hbQ_{\rm op}+g_J\mu_0H(J_z+\gamma I_z), \tag{2}$$

where μ_0 is the Bohr magneton, $Q_{\rm op}$ is the electric-quadrupole operator defined in Ref. 5, and a and b are the magnetic-dipole and electric-quadrupole hyperfine-interaction constants, respectively, and must be determined experimentally. The nuclear spin and electronic angular-momentum operators are denoted by I and J, and I_z and J_z are their projections on the axis of the external field H. The electronic and nuclear g factors are denoted by g_J and g_I, respectively, and are defined by the relations $g_J=-\mu_J/J\mu_0$ and $g_I=-\mu_I/I\mu_0$, where μ_J and μ_I are the dipole moments associated with the spins J and I. The ratio $\gamma=g_I/g_J$ is thus normally of the order of 10^{-3} or less.

The atomic ground state of chromium is $^7S_3$ which arises from the configuration $(3d)^5$ $(4s)^1$. The electronic

[5] N. F. Ramsey, *Molecular Beams* (Oxford University Press, New York, 1956), p. 272.

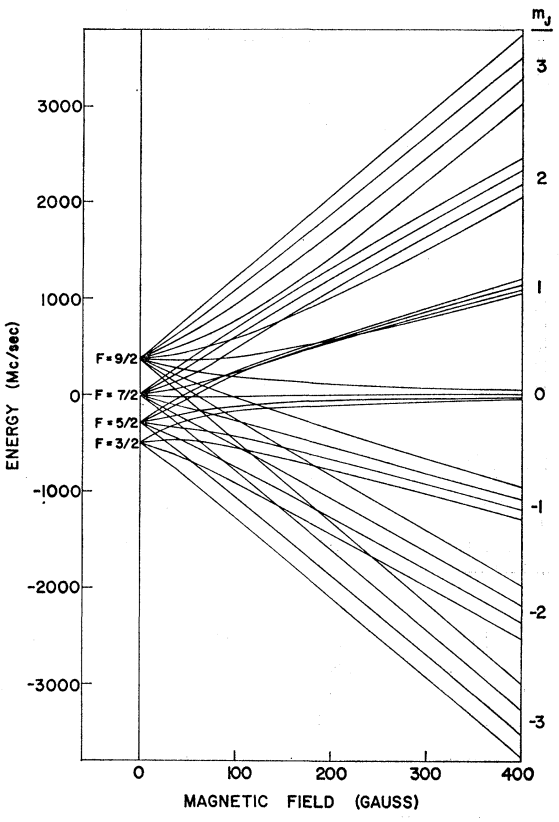

FIG. 4. Hfs diagram (drawn to scale) for Cr^{53}. The magnetic hyperfine-interaction constant a has been assumed positive for simplicity (the sign of a has not been measured). This assumption has no effect on the conclusions reached.

g factor has the measured value[6]

$$g_J = 2.001348 \pm 0.000078.$$

Because this value differs by less than five parts in 10^4 from that expected for an S state, it would appear that the atomic state is a rather pure S state. For this reason, the second term in the Hamiltonian is expected to be very close to 0 (more specifically, b is expected to vanish), although this presumption is subject to test in the present experiment.

Investigation of the nucleus Cr^{53} by a number of investigators[2] has led to the results

$$I(Cr^{53}) = \tfrac{3}{2},$$
$$\mu_I(Cr^{53}) = -0.47437 \text{ nm}.$$

With this information, it is clear that all parameters in the Hamiltonian are known except for a and b, and the latter is expected to be extremely close to 0. The Argonne high-speed digital computer GEORGE was used to calculate eigenvalues and transition frequencies. The quantities in the last column of Table I were calculated with $b=0$ and the value $a=82.5985$ Mc/sec reported in this paper.

Once I and J are known, a qualitative hfs diagram (for $b \approx 0$) can be drawn. From this, it is possible to determine which transitions are observable (i.e., which transitions satisfy the selection rules and the refocusing conditions). Figure 4 is such a hfs diagram. The figure is actually drawn to scale for the measured value of a. Some 51 transitions are "observable." Of these, the 9 actually searched for and seen are indicated by arrows in Fig. 5. The 6 transitions for which precise measurements were obtained are labeled α, β, γ, δ, ϵ, and ζ. It is seen that transitions α, β, and γ are $\Delta F = \pm 1$ single-quantum flop-in transitions. Transitions δ and ϵ are two-quantum $\Delta F = 0$ flop-in transitions, and ζ is a single-quantum flop-out transition. Figures 3 and 6 show the appearance of transitions ζ and α, respectively. In addition to these transitions, 4-quantum and 5-quantum flop-in and 2-quantum flop-out transitions have been observed.

Theoretical Evaluation of the Magnetic Hyperfine-Interaction Constant

The present calculation of the magnetic hyperfine-interaction constant a for chromium I is based on the assumption of pure Russell-Saunders coupling in the $3d^5 4s\ ^7S_3$ ground state. Under this assumption, with the known nuclear spin and magnetic moment for Cr^{53}, it is possible to evaluate the constant a by use of the method of Goudsmit, Fermi, and Segrè as extended by

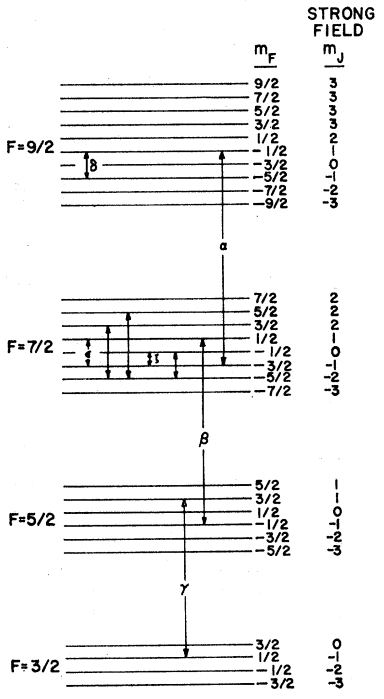

FIG. 5. Schematic hfs diagram at small H for Cr^{53}. All transitions observed are indicated by arrows. The magnetic hfs constant a has been assumed positive.

[6] P. Brix, J. T. Eisinger, H. Lew, and G. Wessel, Phys. Rev. 92, 647 (1953); V. W. Hughes in *Recent Research in Molecular Beams*, edited by I. Estermann (Academic Press Inc., New York, 1959), p. 89.

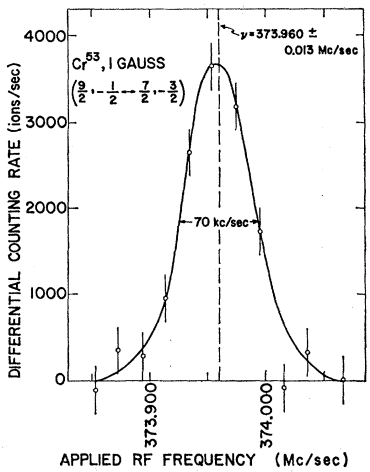

FIG. 6. The $(\frac{9}{2}, -\frac{1}{2} \leftrightarrow \frac{7}{2}, -\frac{3}{2})$ single-quantum flop-in transition α in Cr^{53} as observed at 1 G.

Trees.[7] The result obtained is

$$a(^7S_3) = -119.6\ (1-d\sigma/dn)\ \text{Mc/sec}. \quad (3)$$

The factor $(1-d\sigma/dn)$ describes the rate at which the quantum defect σ changes with the principal quantum number n. The quantum defect is defined (for neutral atoms) by the Rydberg-Ritz equation

$$T = R/(n-\sigma)^2, \quad (4)$$

where

$$\sigma = \alpha + \beta T. \quad (5)$$

In these equations, T denotes the term value (positive for the states of a series, 0 for the limit), and R the Rydberg constant. From Eqs. (4) and (5), it can be shown[8] that

$$d\sigma/dn = \beta(\beta - R^{1/2}/2T^{3/2})^{-1}. \quad (6)$$

The quantity $\beta = d\sigma/dT$ should be a constant for an unperturbed series; it is the slope of the line drawn in Fig. 7, which shows a little curvature near the point $n=4$ which corresponds to the ground state. From the slope of the graph, the value of β at $n=4$ was estimated to be 2.15×10^{-6} cm. With this value it is found from Eq. (6) that $d\sigma/dn = -0.20$.

With this value for $d\sigma/dn$, Eq. (3) gives

$$a_{\text{calc}}(3d^5 4s\ ^7S_3) = -144\ \text{Mc/sec}.$$

Corrections for finite volume of the nucleus and for diamagnetic effects were neglected because they are well below 1% in this case. Because the sign of a has not been measured, only its magnitude can be compared with the measured value $|a(^7S_3)| = 82.5985$ Mc/sec. The large discrepancy between these two values is somewhat surprising and probably is due to our neglect of configuration mixing. The measured values of g_J and b indicate that the mixing configurations are probably those involving the single s-electron excitations either from the inner closed s^2 shells (core excitations) or from the $4s$ shell into the higher unfilled shells up to and including the states of the continuum. The density of the states of the continuum will be large and may well lead to an appreciable contribution to the hyperfine-interaction constant a.

IV. EXPERIMENTAL PROCEDURE

For the chromium runs, about 1g of ordinary chromium metal, in small chunks, was placed in a zirconia oven with a 10-mil slit. On heating the oven to about 1450°C, the chromium beam was easily detected. This could be observed either with or without mechanical square-wave modulation of the beam intensity. After the position and voltages of the universal detector and the position of the oven were optimized, the cold trap of the detector was brought to liquid nitrogen temperature. The inhomogeneous magnets were then set to about 8 kG. Under these conditions, ions from the beam (primarily in the $m_J=0$ state) were detected at a rate of about 7×10^6 sec^{-1} compared with a rest gas background of about 1×10^6 sec^{-1}.

The Cr^{52} resonance, whose frequency is exactly proportional to the strength H of the C field, could be observed at all fields with or without modulation. Its level varied from 1.2 to 2.5×10^6 sec^{-1}. Because the slit in front of the multiplier had been removed, the effective slit width was the full width of the first dynode, about $\frac{1}{2}$ in. For this reason, Cr^{52} and Cr^{53} could be observed simultaneously without any change in the setting of the mass-spectrometer magnet. The Cr^{52} resonance could therefore be used to monitor the C field continuously while accumulating data on Cr^{53}.

Simultaneous observation of transitions in the two isotopes was achieved by feeding the appropriate pair of rf signals into two adjacent loops in the C field. One was used in searching for Cr^{53} transitions while the other was used to hold the field steady through observation

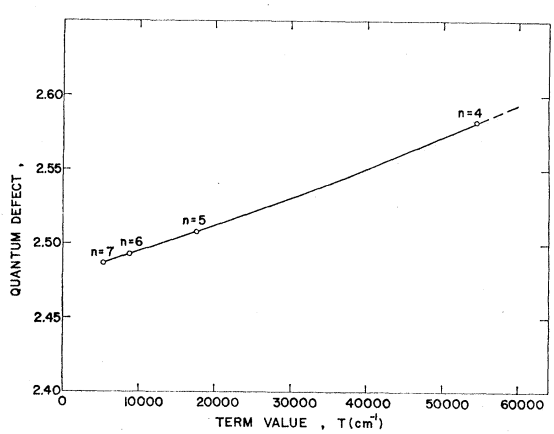

FIG. 7. The quantum defect σ plotted against term value T for the $3d^5_{\frac{1}{2}}\ ns\ ^7S_3$ series in the chromium-I spectrum. Term values were taken from C. E. Moore [*Atomic Energy Levels* (National Bureau of Standards, Washington, D. C., 1952), Vol. 2.]

[7] R. E. Trees, Phys. Rev. **92**, 308 (1953).
[8] M. F. Crawford and A. L. Schawlow, Phys. Rev. **76**, 1310 (1949).

TABLE I. Summary of observations on Cr^{53}.

H (G)	Observed frequency Cr^{52} (Mc/sec)	Cr^{53} Transition $(F, m \leftrightarrow F', m')$	Transition label	N	Type	Observed frequency Cr^{53} (Mc/sec)	$\nu^{53}(\text{obs})-\nu^{53}(\text{calc})$ (kc/sec)
0.417	1.168	$(\frac{9}{2}, -\frac{1}{2} \leftrightarrow \frac{9}{2}, -\frac{5}{2})$	δ	2	flop-in	0.782(7)	3
20.000	56.025	$(\frac{9}{2}, -\frac{1}{2} \leftrightarrow \frac{9}{2}, -\frac{5}{2})$	δ	2	flop-in	38.111(15)	13
20.000	56.025	$(\frac{7}{2}, \frac{1}{2} \leftrightarrow \frac{7}{2}, -\frac{3}{2})$	ϵ	2	flop-in	43.576(10)	10
50.000	140.062	$(\frac{7}{2}, \frac{1}{2} \leftrightarrow \frac{7}{2}, -\frac{3}{2})$	ϵ	2	flop-in	114.435(15)	1
50.000	140.062	$(\frac{7}{2}, -\frac{1}{2} \leftrightarrow \frac{7}{2}, -\frac{3}{2})$	ζ	1	flop-out	116.829(15)	0
1.000	2.801	$(\frac{9}{2}, -\frac{1}{2} \leftrightarrow \frac{7}{2}, -\frac{3}{2})$	α	1	flop-in	373.960(11)	−2
1.000	2.801	$(\frac{7}{2}, \frac{1}{2} \leftrightarrow \frac{5}{2}, -\frac{1}{2})$	β	1	flop-in	291.525(7)	0
1.000	2.801	$(\frac{5}{2}, \frac{3}{2} \leftrightarrow \frac{3}{2}, \frac{1}{2})$	γ	1	flop-in	208.380(7)	3

of the Cr^{52} resonance. The loops were intercalibrated by observing the resonance frequency for the Cr^{52} transition at each loop position and noting the difference.

Once the field was set and held steady with the Cr^{52} signal, the Cr^{53} transitions could be sought. The search normally consisted in counting, with 10 or 30 cps modulation as described above, at each of many adjacent frequencies of the rf. Counting times varied from 30 sec to 5 min.

V. OBSERVATIONS AND MEASUREMENTS

Most of the observations are listed in Table I. The field (in gauss) and the observed Cr^{52} resonance frequency (in Mc/sec), given in columns 1 and 2, respectively, are related by the relation

$$\nu(Cr^{52}) = g_J \mu_0 H/h. \tag{7}$$

The identification and labels of the Cr^{53} transitions are given in columns 3 and 4. In column 3, the quantum numbers given are the values of F and m_F for the state at zero field. Column 5 gives the number N of quanta required for the transition, and column 6 indicates whether, with the present arrangement, the transition should (and does) appear as flop-out or flop-in. The last two columns give the observed resonance frequency (in Mc/sec) for the Cr^{53} transition and the difference (in kc/sec) between this frequency and that calculated theoretically by GEORGE, an Argonne high-speed digital computer. The parameters used for the calculation have been discussed above. The first five observations listed are for $\Delta F = 0$ transitions; the last three are for $\Delta F = \pm 1$ transitions and thus lead directly to an evaluation of the constants a and b.

In addition to the data presented in Table I, several other observations were made at fields between 5 and 10 G. The observations were entirely consistent with those given in the table, but were not made with as great precision.

VI. CONCLUSIONS

At zero magnetic field, the eigenvalues of the hfs Hamiltonian are just the four levels characterized by the F values $\frac{9}{2}$, $\frac{7}{2}$, $\frac{5}{2}$, and $\frac{3}{2}$ as shown at the left in Fig. 4. From the Hamiltonian, the energy differences between these states may be expressed as

$$\begin{aligned} \Delta\nu(\tfrac{9}{2} \leftrightarrow \tfrac{7}{2}) &= \tfrac{9}{2}a + \tfrac{3}{4}b, \\ \Delta\nu(\tfrac{7}{2} \leftrightarrow \tfrac{5}{2}) &= \tfrac{7}{2}a - (7/20)b, \\ \Delta\nu(\tfrac{5}{2} \leftrightarrow \tfrac{3}{2}) &= \tfrac{5}{2}a - \tfrac{3}{4}b. \end{aligned} \tag{8}$$

The measurements of transitions α, β, and γ listed in Table I, corrected to zero field by GEORGE calculations, are

$$\begin{aligned} \Delta\nu(\tfrac{9}{2} \leftrightarrow \tfrac{7}{2}) &= 371.691 \pm 0.011 \text{ Mc/sec}, \\ \Delta\nu(\tfrac{7}{2} \leftrightarrow \tfrac{5}{2}) &= 289.095 \pm 0.007 \text{ Mc/sec}, \\ \Delta\nu(\tfrac{5}{2} \leftrightarrow \tfrac{3}{2}) &= 206.499 \pm 0.007 \text{ Mc/sec}. \end{aligned} \tag{9}$$

When these values are substituted in Eqs. (8), one finds that

$$\begin{aligned} |a(Cr^{53})| &= 82.5985 \pm 0.0015 \text{ Mc/sec}, \\ |b(Cr^{53})| &= 0.003 \pm 0.008 \text{ Mc/sec}. \end{aligned}$$

The constant b is seen to be 0 within experimental error. If b is not 0, it appears to have the opposite sign from a. When, however, b is set equal to 0 and a is re-evaluated, no significant change is found for a, but the fit to the data is worse.

The measured value of $|a|$ has been compared above with the value obtained theoretically according to the procedure of Trees[7] (under the assumption of pure Russell-Saunders coupling).

The term $(ha\mathbf{I}\cdot\mathbf{J})$ in the Hamiltonian is simply a convenient way of representing the interaction of the nuclear magnetic-dipole moment with the magnetic field $\mathbf{H}_J$ which the electronic configuration produces at the nucleus. Thus,

$$ha\mathbf{I}\cdot\mathbf{J} = -\boldsymbol{\mu}_I \cdot \mathbf{H}_J. \tag{10}$$

From this, the internal field is found to be

$$H_J = -(haIJ/\mu_I). \tag{11}$$

When the experimental value $|a(Cr^{53})| = 82.5985$

Mc/sec is used in Eq. (11), it is found that

$$|H_J| = 1.03 \times 10^6 \text{G},$$

with an uncertainty of about 1%. When the theoretical value $a_{\text{calc}}(3d^5 4s\ ^7S_3) = -144$ Mc/sec is used, the same equation gives $H_J = +1.8 \times 10^6$ G.

Freeman and Watson have followed a more detailed approach for the theoretical evaluation of the internal field.[9] They have made approximate spin-polarized Hartree-Fock calculations in which the core electrons are allowed a polarization due to the unpaired $4s$ electron as well as to the unpaired $3d$ electrons. Their result for the $3d^5 4s\ ^7S_3$ configuration gives -0.65×10^6 G from the core polarization and $+1.15 \times 10^6$ G from the $4s$ electron. The internal field is thus calculated to be $+0.50 \times 10^6$ G, a value somewhat closer to the measured value than the simpler estimate given above. Freeman and Watson emphasize that their result for the (present) case of two unfilled shells is especially sensitive to several factors[10] which occur in the calculation.

Although the data suggest that b may be exactly 0, this value is entirely consistent with the data and with what would be expected for a $(d^5 s)$ state.

ACKNOWLEDGMENTS

The authors would like to thank B. Wybourne for valuable discussions concerning the discrepancy between the experimental and theoretical values of a. The authors are equally grateful to A. J. Freeman and R. E. Watson for communication and discussion of their unpublished results. They also thank C. Rush for his ingenious design of the counting circuitry. Valuable contributions to the design and construction of the apparatus were made by J. Dalman, A. Drabik, J. Pernicka, and G. Hoffman.

[9] A. J. Freeman and R. E. Watson (private communication).

[10] R. E. Watson and A. J. Freeman, Phys. Rev. **123**, 2027 (1961).

PHYSICAL REVIEW VOLUME 132, NUMBER 5 1 DECEMBER 1963

Atomic Response Function*

WERNER BRANDT

Department of Physics, New York University, New York, New York

AND

STIG LUNDQVIST

Department of Mathematical Physics, Chalmers University of Technology, Göteborg, Sweden

(Received 30 January 1963; revised manuscript received 6 June 1963)

The response function of atoms is derived approximately within the framework of the time-dependent Hartree scheme for external fields of wavelength large compared to atomic dimensions. Solutions of the resulting dispersion equation correspond to new resonances of atoms. The theory is discussed in terms of the properties of the differential oscillator-strength distribution, or photoabsorption cross section, for the Hartree model and for the statistical model of the atom. An illustrative calculation in the statistical approximation exhibits qualitatively the conditions for the occurrence of these resonances.

INTRODUCTION

CONSIDER an atom in an external field of given frequency ω and of wavelength larger than atomic dimensions. The response of the atom to the field is discussed most conveniently in terms of the properties of its differential oscillator-strength distribution $g(\omega)$. This function is related directly to the photoabsorption cross section of the atom, i.e., the photoextinction coefficient per atom,

$$\sigma(\omega) = (2\pi^2 e^2/mc) g(\omega),$$

where

$$(2\pi^2 e^2/mc) = 8.067 \times 10^{-18} \text{ Ry cm}^2,$$

with $\hbar$ Ry $= 13.6$ eV. Of recent, the need for comprehensive information about the properties of $g(\omega)$ in different frequency ranges for atoms throughout the periodic system has become acute in many fields, and has pointed to the limited description current atomic theory can afford of the response of an atom to an arbitrary external field.

The function $g(\omega)$ may be said to comprise all the fundamental information on the quantum dynamics of atoms. For a cursory survey of the dependence of $g(\omega)$ on frequency and atomic number Z, it is convenient to consider three frequency ranges. In the low-frequency range (1), where $0 \leq (\omega/\text{Ry}) \leq 1$, $g(\omega)$ essentially consists of the sharp lines familiar from optical spectroscopy, separated by frequency ranges of low absorption; in this range, $g(\omega)$ changes irregularly with Z and reflects in its details the atomic binding. In the high-frequency

* The work was supported in part by the U. S. Atomic Energy Commission, the National Aeronautics and Space Administration, the Office of Naval Research, and the Swedish National Research Council.